Letter

Quantum Computation of Hydrogen Bond Dynamics and Vibrational Spectra

Philip Richerme, Melissa C. Revelle, Christopher G. Yale, Daniel Lobser, Ashlyn D. Burch, Susan M. Clark, Debadrita Saha, Miguel Angel Lopez-Ruiz, Anurag Dwivedi, Jeremy M. Smith, Sam A. Norrell, Amr Sabry, and Srinivasan S. Iyengar*

Cite This: *J. Phys. Chem. Lett.* 2023, 14, 7256–7263
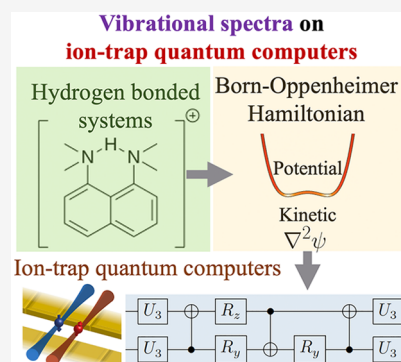
Read Online

ACCESS | Metrics & More | Article Recommendations | Supporting Information

ABSTRACT: Calculating observable properties of chemical systems is often classically intractable and widely viewed as a promising application of quantum information processing. Here, we introduce a new framework for solving generic quantum chemical dynamics problems using quantum logic. We experimentally demonstrate a proof-of-principle instance of our method using the QSCOUT ion-trap quantum computer, where we experimentally drive the ion-trap system to emulate the quantum wavepacket dynamics corresponding to the shared-proton within an anharmonic hydrogen bonded system. Following the experimental creation and propagation of the shared-proton wavepacket on the ion-trap, we extract measurement observables such as its time-dependent spatial projection and its characteristic vibrational frequencies to spectroscopic accuracy (3.3 cm^{-1} wavenumbers, corresponding to >99.9% fidelity). Our approach introduces a new paradigm for studying the chemical dynamics and vibrational spectra of molecules and opens the possibility to describe the behavior of complex molecular processes with unprecedented accuracy.

Vibrational spectra on ion-trap quantum computers

Hydrogen bonded systems → Born-Oppenheimer Hamiltonian (Potential, Kinetic $\nabla^2\psi$)

Ion-trap quantum computers

Hydrogen bonds, hydrogen transfer reactions, and coupled transport of protons/deuterons and electrons are fundamental to many biological, materials, and atmospheric processes.[1−6] Significant challenges influenced by the coupled transport of hydrogen nuclei and electrons include problems in photosynthesis,[7,8] nitrogen fixation,[9] and the anomalous Grotthuss-like behavior in water[10,11] and in fuel cells.[12] Hydrogen bonds and hydrogen transfer reactions are characterized by the interactions of a single hydrogen nucleus confined to a "box" created by electronegative donor and acceptor atoms that regulate the extent to which the interaction is polarized. Since the potential here is inherently anharmonic,[13−17] the commonly used approach of modeling chemical bonds within the harmonic approximation[18,19] is known to drastically fail for hydrogen-bonded systems.[11,13,14,16,20] As a result, calculating the full quantum wavepacket dynamics[13,14,21−28] is often the only approach[13,14] to accurately predict the chemical behavior of such complex problems. Unfortunately, multidimensional quantum nuclear dynamics problems require exponential computational resources[29] to achieve predictive results, forcing existing studies to sacrifice accuracy for efficiency. Solving proton- or hydrogen-transfer dynamics problems using quantum-hardware and quantum-inspired algorithms has also posed a challenge to date. While promising quantum algorithms[30−38] and experiments[39−45] have addressed systems with strongly correlated electrons, these algorithms are incapable of describing quantum nuclear effects within molecules. Likewise, while pioneering work has performed quantum simulations of vibronic spectra[46−49] or wavepacket evolution through conical intersections,[50] these studies have been limited to molecular potentials approximated as harmonic (inapplicable to hydrogen-bonded systems) and evaluated at a single molecular geometry.

Here, we introduce a suite of techniques for performing accurate quantum nuclear dynamics calculations on a single Born–Oppenheimer potential energy surface by using quantum hardware. Our approach exploits the fact that the quantum nuclear dynamics problems may contain far fewer than $O(4^N)$ independent elements when represented as a $2^N \times 2^N$ matrix, requiring a dramatically reduced number of operations when mapped to quantum simulation hardware.[51] In this work, we demonstrate this idea and focus on mapping simple one-dimensional hydrogen-bond systems onto quantum hardware.
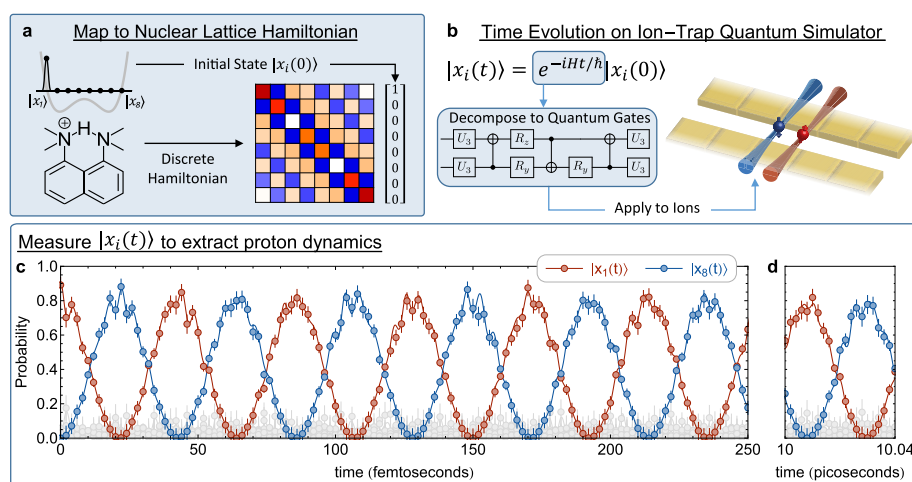
Figure 1. Coherent dynamics of a shared-proton wavepacket. (a) The quantum dynamics of a short-strong hydrogen bonded system are mapped onto a discrete basis. Each basis state represents a shared-proton wavepacket occupying one of the equally spaced lattice sites between the donor/acceptor frameworks. The discrete Hamiltonian is formed from writing the kinetic and potential energy operators for the shared-proton in this system. (b) Time evolution under the nuclear Hamiltonian is achieved by applying a unitary propagator to an initial wavepacket state. The unitary operator is decomposed into single- and two-qubit quantum gates that are applied to a trapped-ion quantum computer. (c) The quantum dynamics of the trapped-ion system emulate those of the shared proton wavepacket. When a wavepacket is initialized near the left side of the anharmonic potential well, its dynamics are found to oscillate coherently between the donor and acceptor groups. Solid lines show the exact numerical solution to the Schrödinger equation, including decoherence effects. (d) Our trapped-ion experiment remains coherent for many hundreds of emulated shared-proton oscillations with no visible reduction in contrast.

To provide a proof-of-principle of our approach, we emulate the time dynamics of a shared-proton wavepacket evolving within a hydrogen-bonded system[52] using a two-qubit quantum computer. For specificity, we choose an exemplar molecule, monoprotonated bis(1,8-dimethylamino)-naphthalene (DMANH$^+$), which has a shared proton bound by a smooth, symmetric, double-well potential spanning the donor–acceptor range and exhibits a structure common to many strong hydrogen-bonded systems. Our experiment implements the effective nuclear Hamiltonian of this hydrogen bonded system by mapping it to a trapped-ion quantum computer with site-specific preparation, control, and readout.[53] We apply discrete quantum logic gates to drive the system's unitary time evolution from which we directly determine the spatial and temporal projection of the shared-proton wavepacket, its characteristic vibrational (anharmonic) frequencies, and the energy eigenspectrum of the applied nuclear Hamiltonian. Our experiment shows exceptional agreement with the corresponding classical calculations of the shared-proton vibrational and energy spectra for this model problem, with a 0.1% uncertainty (≈ 3 cm^{-1} error in the resultant vibrational spectrum). The experimental techniques described here are directly scalable to larger numbers of qubits and, following the framework we introduce below, may be applied to study more complex chemical problems with multiple nuclear degrees of freedom.

The general problem of quantum chemical dynamics is complicated by two primary challenges: (a) The classical computational cost associated with obtaining accurate electronic potential energy surfaces may grow exponentially with the number of nuclear degrees of freedom.[14,54−56] (b) Both the classical storage of the quantum unitary propagator and quantum wavepackets, as well as the time-evolution of the propagator acting on the quantum states, may also require exponential resources with system size.[56−61] In this Letter, we present a framework which directly addresses challenge (b) by

expressing generic nuclear Hamiltonians in a form amenable to implementation on quantum hardware. Specifically, we show how the nuclear dynamics on a single Born–Oppenheimer potential energy surface may be mapped to an interacting configuration of quantum bits, as may be found in spin–lattice quantum simulators or universal quantum computers.

For both classical- and quantum-computational approaches to studying chemical dynamics problems, the initial step is to express the nuclear Hamiltonian in some suitable basis, such as a discrete coordinate basis (Figure 1a) that is commonly used in quantum dynamics studies.[21,23−25,28,62,63] In our study, we interpolate a lattice of 2^N equally spaced points between the donor/acceptor groups and then choose a set of 2^N basis functions corresponding to Dirac delta-functions centered on those lattice sites. The shape of the shared-proton wavepacket at any time is thus represented by a ket vector, with its time dependence governed by unitary Schrödinger evolution under the system Hamiltonian.

In this discrete basis, the diagonal elements of the shared-proton Hamiltonian encode an effective double-well potential energy surface arising from the surrounding nuclear frameworks and electronic structure. This potential energy surface, local in the coordinate representation, includes explicit electron correlation and is treated here by using density functional theory. For a specific molecular system, the calculated shape of the double-well potential depends upon the level of electronic structure theory used to depict electron correlation as well as the chosen grid spacing used to represent the nuclear degrees of freedom. The off-diagonal elements of the shared-proton Hamiltonian encode the nuclear kinetic energy and are determined here using distributed approximating functionals (DAFs).[51,64−66] Underlying symmetries in the nuclear Hamiltonian allow it to be written in a form more amenable for efficient experimental realizations.[51] The symmetric double-well potential seen by the shared-proton wavepacket, for instance, leads to reflection symmetry in the
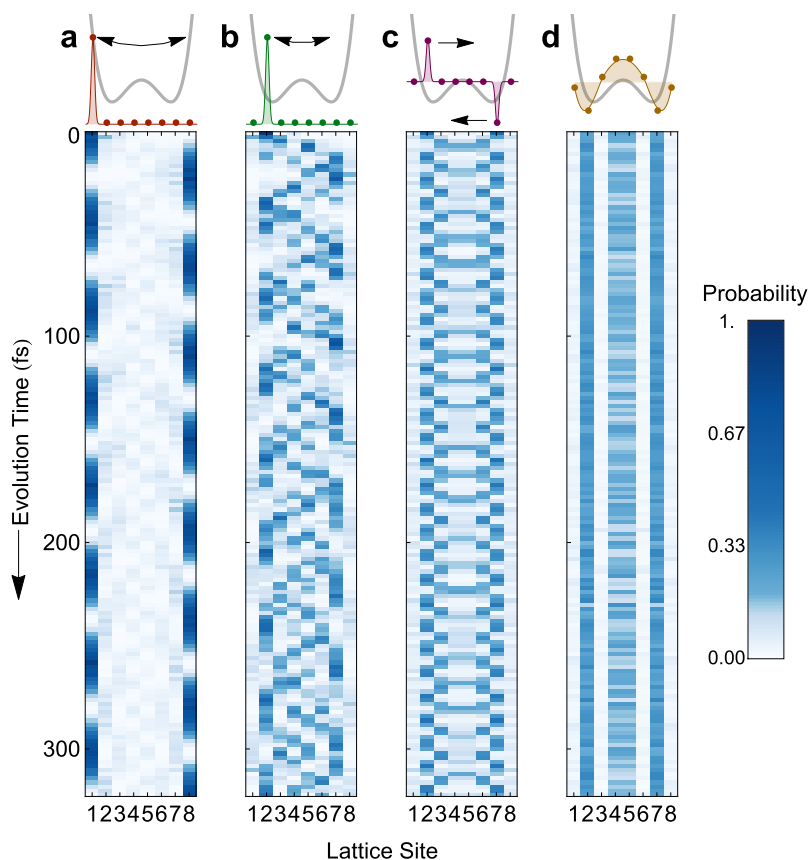
Figure 2. Experimentally determined dynamics of a shared proton in DMANH$^+$. The observed time evolution depends on whether the shared-proton wavepacket is initialized (a) near the donor site; (b) near one of the potential energy surface minima; (c) split between the two minima with opposite phase; or (d) in an eigenstate of the double-well potential. Oscillations in both space and time are observed in all cases, except in panel d, where the system remains in its eigenstate.

diagonal elements of the Hamiltonian. In addition, the kinetic energy operator of the shared-proton wavepacket, when represented using DAFs, imprints a Toeplitz structure to the off-diagonal elements for which each subdiagonal has a constant value. Matrices with these key properties can be transformed into a block-diagonal form by applying a Givens rotation operation to the computational basis.[51] The net effect of this mapping is to recast the original $2^N \times 2^N$ nuclear Hamiltonian as one with two sub-blocks of dimension $2^{N-1} \times 2^{N-1}$, with each sub-block operating independently on half of the Hilbert space. Thus, the time-evolution of the full Hamiltonian can be implemented by performing time-evolution of both subblocks independently and then applying an inverse mapping to transform back to the original basis. In Supporting Information, we discuss two approaches for implementing the time evolution on a collection of interacting quantum bits. In one case we provide a control map[51,67] that directly encodes the molecular Hamiltonian onto an ion-trap Hamiltonian. This approach was introduced in ref 51. Alternately, in this Letter, each sub-block of the unitary propagator is directly decomposed into a sequence of single- and two-qubit gates for implementation on a universal quantum computer.

To emulate the chemical dynamics of this hydrogen-bonded system, lasers are used to prepare and manipulate the internal electronic states of trapped atomic ions (Figure 1b). Qubit levels are encoded in the $^2S_{1/2}$ $|F = 0, m_F = 0\rangle$ and $|F = 1, m_F = 0\rangle$ hyperfine "clock" states of ^{171}Yb$^+$ ions, denoted $|0\rangle$ and $|1\rangle$,

respectively.[68] State preparation proceeds by optically pumping all qubits to $|0\rangle$ and then performing local rotations to generate a state corresponding to an initial shared-proton wavepacket. To find the shared-proton wavepacket at a later time t, we time-evolve the initial state under the unitary propagator $U(t) = e^{-iHt/\hbar}$, where H is the ion-trap Hamiltonian that encodes the effective nuclear dynamics. While H is generically expressed in terms of Ising-type XX and YY interactions,[51] here we exploit the small system size to optimally decompose the propagator $U(t) = e^{-iHt/\hbar}$ into a sequence of seven single-qubit rotations (with time-dependent angles) and three controlled-NOT (CNOT) gates.[69−72] The details of the decomposition scheme can be found in the Supporting Information.

We generate single- and two-qubit gates by applying spin-dependent optical dipole forces to ions confined in a surface-electrode trap (Sandia HOA-2.1[73]). Each ion is addressed by two laser beams near 355 nm: one tightly focused individual-addressing beam and one global beam that targets all ions simultaneously. The beams are arranged such that their wavevector difference $\vec{\Delta k}$ lies along the transverse principal axes in plane with the trap surface. The two beams contain frequency components whose difference can be matched to the resonant transition of the ion qubit at ν_0 = 12.642819 GHz to drive single-qubit gates, or detuned symmetrically from ν_0 to drive Mølmer−Sørensen two-qubit interactions. Gate times for single-qubit $\pi/2$ flips are typically 10 μs with 99.5% fidelity, while typical Mølmer−Sørensen gates require 200 μs for full entanglement with a typical 97% fidelity.
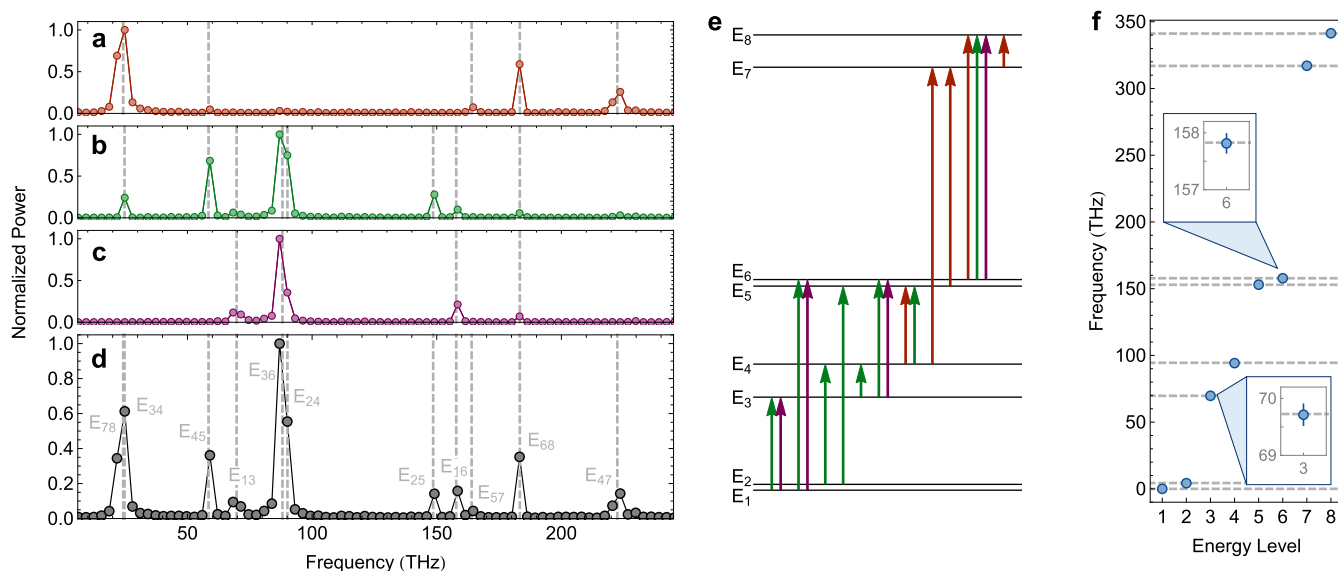
Figure 3. Experimentally determined frequency and energy spectra of a shared-proton in DMANH$^+$. (a−c) The time evolution data for the initial states in Figure 2a−c are Fourier-transformed to reveal frequency spectra of the shared-proton oscillation. Each peak corresponds to a frequency splitting between eigenstates of the discrete nuclear Hamiltonian. (d) The data in panels a−c are summed to produce a final frequency spectrum. Dashed gray lines and labels show predicted frequencies from exact diagonalization of the nuclear Hamiltonian. (e) The extracted frequencies from panels a−d, color-coded by their parent spectrum, allow the relative energies of all eigenstates to be experimentally determined. (f) The quantum-computed energy eigenstates of the nuclear Hamiltonian (blue dots) are compared to the exact-diagonalization result (dashed gray lines). Typical error bars (1 s.d.) are shown in the insets.

After initialization of the ion qubits and application of gates to simulate Hamiltonian evolution for time t, the qubit states are measured to determine the time-evolved shape of the shared-proton wavepacket. At each time step, measurements of the trapped-ion qubit states determine the probability of finding the shared-proton on each of the 2^N lattice sites. Detection of the final ion states is accomplished by capturing their spin-dependent fluorescence into a fiber array, where each fiber is coupled to an individual photomultiplier-tube (PMT). Site-resolved detection allows for discrimination of each qubit's logical $|0\rangle$ or $|1\rangle$ states with 99.0% detection fidelity, as well as the probability overlap with all possible basis states. Experiments are repeated 1000 times at each time step to limit the statistical error contributions from quantum projection noise. The time-dependent proton dynamics is then determined by mapping the observed ion dynamics back to the discrete proton basis. More details of the experimental setup and implementation can be found in the Supporting Information.

In Figure 1c, we highlight the probabilities of finding the shared-proton on the leftmost ($|x_1\rangle$) and rightmost ($|x_8\rangle$) lattice sites on the potential energy surface when it is initialized in the $|x_1\rangle$ position. For this initial state, the shared-proton wavepacket is found to exhibit large-amplitude, coherent oscillations between the donor/acceptor groups as well as smaller-amplitude, higher-frequency oscillations; intermediate lattice sites contribute negligibly to the dynamics in this case (gray points in Figure 1c). We emphasize that the solid lines in Figure 1c are not fits to the data; rather, they are an exact numerical solution to the Schrödinger equation in the presence of known quantum gate infidelities.

In our experiments, the quantum circuit in Figure 1b is implemented with ~90% fidelity for any simulated evolution time t. This results in effective shared-proton oscillations that remain coherent for arbitrarily long times with no apparent

decrease in contrast. Figure 1d shows a continuation of the dynamics from Figure 1c, with hundreds of oscillation periods after the wavepacket is initialized. Remarkably, since the gate errors are the same for each time step, they do not affect the frequency information encoded in the time dynamics. For instance, we show below that the shared-proton vibrational frequencies may be determined to >99.9% accuracy despite the ~90% overall circuit fidelity (see SI Sections S.V and S.VI).

Initializing our system in different quantum states, which corresponds to initializing the shared-proton wavepacket on different lattice sites, leads to a variety of different time-dependent oscillations. In Figure 2a, the effective shared-proton state is initialized to occupy the left-most lattice site at $t = 0$. Just as in Figure 1c,d, the time dynamics reveal wavepacket jumps between the $|x_1\rangle$ and $|x_8\rangle$ lattice sites at a rate of ~24 THz (800 cm^{-1}). In contrast, when the shared-proton state is initialized on the second lattice site (Figure 2b), a continuous oscillation between sites $|x_2\rangle$ through $|x_7\rangle$ is observed with nearly zero probability of occupying the extrema ($|x_1\rangle$ and $|x_8\rangle$). When positive and negative wavepacket components are introduced in the left and right wells (respectively), as in Figure 2c, strong oscillations are observed along with destructive interference effects near the center of the double well potential. Finally, when the initial proton wavepacket is prepared in an eigenstate of the nuclear Hamiltonian (Figure 2d), no time-dependent dynamics are expected or observed.

Our emulation of the shared-proton wavepacket dynamics enables a high-accuracy determination of its vibrational frequencies. Consider the nuclear Hamiltonian H, which has eigenstates $\phi_i(x)$ and energy eigenvalues E_i. Any chosen initial state $\chi(x, 0)$ may be written in terms of this eigenstate basis with corresponding time evolution:

$$\chi(x, t) = \sum_i c_i(0)e^{-iE_i t/\hbar}\phi_i(x) \tag{1}$$

Hence, the probability of finding the shared proton at position x at time t is given by

$$|\chi(x, t)|^2 = \sum_{i,j} c_j^*(0)c_i(0)e^{i(E_j - E_i)t/\hbar}\phi_j^*(x)\phi_i(x) \tag{2}$$

The time evolution of any initial state therefore is comprised of oscillations at all possible frequency differences between all pairs of energy eigenstates. For each frequency component, the strength is governed by the product of overlap amplitudes $c_j^*(0)c_i(0)$, that is, the coefficients comprising the initial wavepacket.

To extract the oscillation frequencies of the shared-proton wavepacket in our hydrogen-bonded system, we perform a Fourier transform of the measured time-evolution data presented in Figure 2. Mathematically, this operation is equivalent to taking

$$\int e^{i\omega t}|\chi(x, t)|^2 dt = \sum_{i,j}\left[\int e^{i\omega t}e^{i(E_j - E_i)t/\hbar}dt\right]c_j^*c_i\phi_j^*(x)\phi_i(x)$$

$$= \sum_{i,j}\delta(\omega - (E_j - E_i)/\hbar)c_j^*c_i\phi_j^*(x)\phi_i(x) \tag{3}$$

which produces peaks in the Fourier spectrum corresponding to frequency differences between energy eigenstates, $(E_j - E_i)/\hbar$. This expression is also related to the Fourier transform of the density matrix autocorrelation function, $\text{Tr}[\rho(0)\rho(t)]$, and this aspect is discussed in the Supporting Information, Sections S.V and S.VI.

Fourier transforms of the shared-proton time dynamics (Figure 2a−c) are shown in Figure 3a−c, along with a cumulative spectrum in Figure 3d. The extracted peaks provide a direct measurement of the energy eigenstate differences $E_{ij} \equiv (E_j - E_i)$, which show excellent agreement with the frequencies predicted from exact diagonalization of the nuclear Hamiltonian (gray dashed lines in Figure 3a−d). Note that since the initial wavepacket state in Figure 2d was prepared in an eigenstate and contains minimal time dynamics, its Fourier transform contains no meaningful frequency information.

Using the measured energy differences E_{ij} in Figure 3a−d, we experimentally reconstruct the full energy eigenspectrum of our nuclear Hamiltonian. Since the shared-proton basis has been discretized onto 8 lattice sites, our Hamiltonian contains 8 energy eigenvalues which are calculable and drawn to scale in Figure 3e. The set of measurements $\{E_{ij}\}$ from Figure 3a−d provides more information than is necessary to determine the relative spacings of all energy levels. This overcompleteness arises from our multiple different wavepacket initializations, and it allows for multiple independent measurements of specific energy splittings and reduced error in our final results.

The vibrational energies obtained directly from the ions' time dynamics are compared in Figure 3f to the exact diagonalization results (dashed gray lines). Exceptional agreement is found in all cases. Typical measurement uncertainties are at the level of 0.1%, which corresponds to 3.3 cm^{-1} wavenumbers and is well within the range of spectroscopic accuracy for such molecular vibration problems.

Thus, this Letter presents a rigorous theoretical framework and experimental demonstration for treating general chemical dynamics problems using quantum hardware. We have shown how molecular systems with anharmonic potential energy landscapes, such as the ubiquitous hydrogen bond, may be mapped to a system of controllable interacting quantum bits. We have performed a proof-of-principle demonstration of our mapping, finding excellent agreement between the observed hydrogen-bond dynamics and extracted spectra compared with those calculated on classical hardware. Finally, we discussed an outlook toward extending our approach to more complex chemical systems with multiple correlated nuclear degrees of freedom.

We remark that our experimental technique for extracting all energy eigenvalues of a many-body Hamiltonian has yielded higher accuracies (by nearly two orders-of-magnitude) than previous efforts using trapped-ion quantum systems.[74,75] We note that this high accuracy is driven by the resilience of frequency information in our time-series data despite accumulated quantum gate errors at the ∼10% level. Our observations establish that current-generation, noisy quantum hardware can already serve as a precise computational resource for studying the spectral features of many-body Hamiltonians.

We have for the first time demonstrated that generalized nuclear dynamics can be modeled exactly using a qubit-based quantum processor. This is a marked departure from the existing literature, where vibrations within the harmonic approximation are mapped to Bosonic systems. Building on the high-accuracy quantum simulations presented here, we will broaden our implementation to include multiple correlated nuclear degrees of freedom within the nuclear Hamiltonian to capture more realistic wavepacket trajectories across the potential energy surface and also allow for Boltzmann averaging over thermally fluctuating donor−acceptor distances. Ultimately, we expect to compare and validate our quantum-computed results with experiments performed by gas-phase spectroscopy, for which the Hamiltonian description of an isolated nuclear wavepacket is most appropriate.

■ ASSOCIATED CONTENT

ⓈI Supporting Information

The Supporting Information is available free of charge at https://pubs.acs.org/doi/10.1021/acs.jpclett.3c01601.

> Additional details regarding the mapping framework between ion-trap systems and chemical dynamics Hamiltonians, details of the QSCOUT ion-trap experimental setup, and methods for computing molecular vibrational spectra from ion-trap measurements (PDF)

■ AUTHOR INFORMATION

Corresponding Author

Srinivasan S. Iyengar − *Quantum Science and Engineering Center and Department of Chemistry, Indiana University, Bloomington, Indiana 47405, United States;* ⓘ orcid.org/0000-0001-6526-2907; Email: iyengar@indiana.edu

Authors

Philip Richerme − *Department of Physics, Indiana University, Bloomington, Indiana 47405, United States; Quantum Science and Engineering Center, Indiana University, Bloomington, Indiana 47405, United States*

Melissa C. Revelle − *Sandia National Laboratories, Albuquerque, New Mexico 87123, United States*

Christopher G. Yale − *Sandia National Laboratories, Albuquerque, New Mexico 87123, United States*

Daniel Lobser − *Sandia National Laboratories, Albuquerque, New Mexico 87123, United States*

Ashlyn D. Burch − *Sandia National Laboratories, Albuquerque, New Mexico 87123, United States*

Susan M. Clark − *Sandia National Laboratories, Albuquerque, New Mexico 87123, United States*

Debadrita Saha − *Department of Chemistry, Indiana University, Bloomington, Indiana 47405, United States*

Miguel Angel Lopez-Ruiz − *Department of Chemistry, Indiana University, Bloomington, Indiana 47405, United States*

Anurag Dwivedi − *Department of Chemistry, Indiana University, Bloomington, Indiana 47405, United States*

Jeremy M. Smith − *Department of Chemistry, Indiana University, Bloomington, Indiana 47405, United States;* 🄾 orcid.org/0000-0002-3206-4725

Sam A. Norrell − *Department of Physics, Indiana University, Bloomington, Indiana 47405, United States*

Amr Sabry − *Quantum Science and Engineering Center and Department of Computer Science, Indiana University, Bloomington, Indiana 47405, United States*

Complete contact information is available at:
https://pubs.acs.org/10.1021/acs.jpclett.3c01601

Notes

The authors declare no competing financial interest.

◼ REFERENCES

(1) Hynes, J. T., Klinman, J. P., Limbach, H.-H., Schowen, R. L., Eds.; *Hydrogen-Transfer Reactions*; Wiley-VCH: Weinheim, Germany, 2007.

(2) Breslow, R. Hydrophobic Effects On Simple Organic-Reactions In Water. *Acc. Chem. Res.* **1991**, *24*, 159−164.

(3) Jung, Y.; Marcus, R. A. On The Theory Of Organic Catalysis On Water. *J. Am. Chem. Soc.* **2007**, *129*, 5492−5502.

(4) Yano, J.; Yachandra, V. *Mn₄Ca* cluster in photosynthesis: where and how water is oxidized to dioxygen. *Chem. Rev.* **2014**, *114*, 4175−4205.

(5) Lubitz, W.; Chrysina, M.; Cox, N. Water oxidation in photosystem II. *Photosynth. Res.* **2019**, *142*, 105−125.

(6) Frey, P. A.; Whitt, S. A.; Tobin, J. B. A Low-Barrier Hydrogen-Bond in the Catalytic Triad of Serine Proteases. *Science* **1994**, *264*, 1927.

(7) Alstrum-Acevedo, J. H.; Brennaman, M. K.; Meyer, T. J. Chemical Approaches to Artificial Photosynthesis. 2. *Inorg. Chem.* **2005**, *44*, 6802.

(8) You, B.; Jiang, N.; Sheng, M.; Gul, S.; Yano, J.; Sun, Y. High-Performance Overall Water Splitting Electrocatalysts Derived from Cobalt-Based Metal-Organic Frameworks. *Chem. Mater.* **2015**, *27*, 7636−7642.

(9) Harris, D. F.; Lukoyanov, D. A.; Shaw, S.; Compton, P.; Tokmina-Lukaszewska, M.; Bothner, B.; Kelleher, N.; Dean, D. R.; Hoffman, B. M.; Seefeldt, L. C. The Mechanism of N_2 Reduction Catalyzed by Fe-Nitrogenase Involves Reductive Elimination of H_2. *Biochemistry* **2018**, *57*, 701−710.

(10) Agmon, N. The Grotthuss Mechanism. *Chem.Phys.Lett.* **1995**, *244*, 456.

(11) Shin, J.-W.; Hammer, N. I.; Diken, E. G.; Johnson, M. A.; Walters, R. S.; Jaeger, T. D.; Duncan, M. A.; Christie, R. A.; Jordan, K. D. Infrared Signature of Structures Associated with the $H^+(H_2O)_n$ (N = 6 to 27) Clusters. *Science* **2004**, *304*, 1137.

(12) Knox, C. K.; Voth, G. A. Probing Selected Morphological Models of Hydrated Nation Using Large-Scale Molecular Dynamics Simulations. *J. Phys. Chem. B* **2010**, *114*, 3205.

(13) Vendrell, O.; Gatti, F.; Meyer, H.-D. Dynamics and Infrared Spectroscopy of the Protonated Water Dimer. *Ang. Chem. Int. Ed.* **2007**, *46*, 6918.

(14) Sumner, I; Iyengar, S. S. Quantum Wavepacket Ab Initio Molecular Dynamics: An Approach for Computing Dynamically Averaged Vibrational Spectra Including Critical Nuclear Quantum Effects. *J. Phys. Chem. A* **2007**, *111*, 10313.

(15) Roscioli, J. R.; McCunn, L. R.; Johnson, M. A. Quantum Structure of the Intermolecular Proton Bond. *Science* **2007**, *316*, 249.

(16) Li, X.; Oomens, J.; Eyler, J. R.; Moore, D. T.; Iyengar, S. S. Isotope Dependent, Temperature Regulated, Energy Repartitioning in a Low-Barrier, Short-Strong Hydrogen Bonded Cluster. *J. Chem. Phys.* **2010**, *132*, 244301.

(17) Kamarchik, E.; Mazziotti, D. A. Coupled nuclear and electronic ground-state motion from variational reduced-density-matrix theory with applications to molecules with floppy or resonant hydrogens. *Phys. Rev. A* **2009**, *79*, 012502.

(18) Pople, J. A.; Raghavachari, K.; Schlegel, H. B.; Binkley, J. S. Derivative Studies in Hartree-Fock and Møller-Plesset Theories. *Int. J. Quantum Chem., Quant. Chem. Symp.* **1979**, *16*, 225−241.

(19) Pople, J. A.; Schlegel, H. B.; Raghavachari, K.; DeFrees, D. J.; Binkley, J. S.; Frisch, M. J.; Whiteside, R. A.; Hout, R. F.; Hehre, W. J. Molecular orbital studies of vibrational frequencies. *Int. J. Quantum Chem., Quant. Chem. Symp.* **1981**, *20*, 269−278.

(20) Headrick, J. M.; Diken, E. G.; Walters, R. S.; Hammer, N. I.; Christie, R. A.; Cui, J.; Myshakin, E. M.; Duncan, M. A.; Johnson, M. A.; Jordan, K. Spectral Signatures of Hydrated Proton Vibrations in Water Clusters. *Science* **2005**, *308*, 1765.

(21) Feit, M. D.; Fleck, J. A. Solution of the Schrödinger Equation by a Spectral Method II: Vibrational Energy Levels of Triatomic Molecules. *J. Chem. Phys.* **1983**, *78*, 301.

(22) Schatz, G. C. Quantum Effects in Gas Phase Bimolecular Chemical Reactions. *Annu. Rev. Phys. Chem.* **1988**, *39*, 317.

(23) Leforestier, C.; Bisseling, R. H.; Cerjan, C.; Feit, M. D.; Friesner, R.; Guldberg, A.; Hammerich, A.; Jolicard, D.; Karrlein, W.; Meyer, H. D.; Lipkin, N.; Roncero, O.; Kosloff, R. A Comparison of Different Propagation Schemes for the Time-Dependent Schrödinger Equation. *J. Comput. Phys.* **1991**, *94*, 59.

(24) Tal-Ezer, H.; Kosloff, R. An accurate and efficient scheme for propagating the time dependent Schrödinger equation. *J. Chem. Phys.* **1984**, *81*, 3967.

(25) Gray, S. K.; Balint-Kurti, G. G. Quantum Dynamics with Real Wave Packets, Including Application to Three-Dimensional (J = 0) D +H_2 → HD+H Reactive Scattering. *J. Chem. Phys.* **1998**, *108*, 950.

(26) Meyer, H. D.; LeQuere, F.; Leonard, C.; Gatti, F. Calculation and Selective Population of Vibrational Levels with the Multi-configuration Time-Dependent Hartree (MCTDH) Algorithm. *Chem. Phys.* **2006**, *329*, 179.

(27) Iyengar, S. S.; Kouri, D. J.; Hoffman, D. K. Particular and Homogeneous Solutions of Time-Independent Wavepacket Schrödinger Equations: Calculations Using a Subset of Eigenstates of Undamped or Damped Hamiltonians. *Theor. Chem. Acc.* **2000**, *104*, 471.

(28) Huang, Y.; Iyengar, S. S.; Kouri, D. J.; Hoffman, D. K. Further Analysis of Solutions to the Time-Independent Wavepacket Equations of Quantum Dynamics II: Scattering As a Continuous Function of Energy Using Finite, Discrete Approximate Hamiltonians. *J. Chem. Phys.* **1996**, *105*, 927.

(29) Feynman, R. P. Simulating physics with computers. *International Journal of Theoretical Physics* **1982**, *21*, 467−488.

(30) Abrams, D. S.; Lloyd, S. Simulation of many-body Fermi systems on a universal quantum computer. *Phys. Rev. Lett.* **1997**, *79*, 2586.

(31) Aspuru-Guzik, A.; Dutoi, A. D.; Love, P. J.; Head-Gordon, M. Simulated quantum computation of molecular energies. *Science* **2005**, *309*, 1704.

(32) Wang, H.; Kais, S.; Aspuru-Guzik, A.; Hoffmann, M. R. Quantum algorithm for obtaining the energy spectrum of molecular systems. *Phys. Chem. Chem. Phys.* **2008**, *10*, 5388−5393.

(33) Wecker, D.; Hastings, M. B.; Troyer, M. Progress towards practical quantum variational algorithms. *Phys. Rev. A* **2015**, *92*, 042303.

(34) McClean, J. R.; Romero, J.; Babbush, R.; Aspuru-Guzik, A. The theory of variational hybrid quantum-classical algorithms. *New J. Phys.* **2016**, *18*, 023023.

(35) O'Malley, P. J. J.; Babbush, R.; Kivlichan, I. D.; Romero, J.; McClean, J. R.; Barends, R.; Kelly, J.; Roushan, P.; Tranter, A.; Ding, N.; Campbell, B.; Chen, Y.; Chen, Z.; Chiaro, B.; Dunsworth, A.; Fowler, A. G.; Jeffrey, E.; Lucero, E.; Megrant, A.; Mutus, J. Y.; Neeley, M.; Neill, C.; Quintana, C.; Sank, D.; Vainsencher, A.; Wenner, J.; White, T. C.; Coveney, P. V.; Love, P. J.; Neven, H.; Aspuru-Guzik, A.; Martinis, J. M. Scalable Quantum Simulation of Molecular Energies. *Phys. Rev. X* **2016**, *6*, 031007.

(36) Parrish, R. M.; Hohenstein, E. G.; McMahon, P. L.; Martinez, T. J. Quantum Computation of Electronic Transitions Using a Variational Quantum Eigensolver. *Phys. Rev. Lett.* **2019**, *122*, 230401.

(37) Zhang, J. H.; Iyengar, S. S. Graph-|Q⟩⟨C|: A Graph-based Quantum-classical algorithm for efficient electronic structure on hybrid quantum/classical hardware systems: Improved quantum circuit depth performance. *J. Chem. Theory Comput.* **2022**, *18*, 2885.

(38) Smart, S. E.; Mazziotti, D. A. Quantum solver of contracted eigenvalue equations for scalable molecular simulations on quantum computing devices. *Phys. Rev. Lett.* **2021**, *126*, 070504.

(39) Lanyon, B. P.; Whitfield, J. D.; Gillett, G. G.; Goggin, M. E.; Almeida, M. P.; Kassal, I.; Biamonte, J. D.; Mohseni, M.; Powell, B. J.; Barbieri, M.; Aspuru-Guzik, A.; White, A. G. Towards quantum chemistry on a quantum computer. *Nature Chem.* **2010**, *2*, 106−111.

(40) Lu, D.; Xu, N.; Xu, R.; Chen, H.; Gong, J.; Peng, X.; Du, J. Simulation of chemical isomerization reaction dynamics on a NMR quantum simulator. *Phys. Rev. Lett.* **2011**, *107*, 020501.

(41) Peruzzo, A.; McClean, J.; Shadbolt, P.; Yung, M.-H.; Zhou, X.-Q.; Love, P. J.; Aspuru-Guzik, A.; O'brien, J. L. A variational eigenvalue solver on a photonic quantum processor. *Nat. Commun.* **2014**, *5*, 4213.

(42) Kandala, A.; Mezzacapo, A.; Temme, K.; Takita, M.; Brink, M.; Chow, J. M.; Gambetta, J. M. Hardware-efficient variational quantum eigensolver for small molecules and quantum magnets. *Nature* **2017**, *549*, 242.

(43) Hempel, C.; Maier, C.; Romero, J.; McClean, J.; Monz, T.; Shen, H.; Jurcevic, P.; Lanyon, B. P.; Love, P.; Babbush, R.; Aspuru-Guzik, A.; Blatt, R.; Roos, C. F. Quantum Chemistry Calculations on a Trapped-Ion Quantum Simulator. *Phys. Rev. X* **2018**, *8*, 031022.

(44) Nam, Y.; Chen, J.-S.; Pisenti, N. C.; Wright, K.; Delaney, C.; Maslov, D.; Brown, K. R.; Allen, S.; Amini, J. M.; Apisdorf, J.; Beck, K. M.; Blinov, A.; Chaplin, V.; Chmielewski, M.; Collins, C.; Debnath, S.; Hudek, K. M.; Ducore, A. M.; Keesan, M.; Kreikemeier, S. M.; Mizrahi, J.; Solomon, P.; Williams, M.; Wong-Campos, J. D.;

Moehring, D.; Monroe, C.; Kim, J. Ground-state energy estimation of the water molecule on a trapped-ion quantum computer. *npj Quantum Inf* **2020**, *6*, 33.

(45) Arute, F.; Arya, K.; Babbush, R.; Bacon, D.; Bardin, J. C.; Barends, R.; Boixo, S.; Broughton, M.; Buckley, B. B.; Buell, D. A.; Burkett, B.; Bushnell, N.; Chen, Y.; Chen, Z.; Chiaro, B.; Collins, R.; Courtney, W.; Demura, S.; Dunsworth, A.; Farhi, E.; Fowler, A.; Foxen, B.; Gidney, C.; Giustina, M.; Graff, R.; Habegger, S.; Harrigan, M. P.; Ho, A.; Hong, S.; Huang, T.; Huggins, W. J.; Ioffe, L.; Isakov, S. V.; Jeffrey, E.; Jiang, Z.; Jones, C.; Kafri, D.; Kechedzhi, K.; Kelly, J.; Kim, S.; Klimov, P. V.; Korotkov, A.; Kostritsa, F.; Landhuis, D.; Laptev, P.; Lindmark, M.; Lucero, E.; Martin, O.; Martinis, J. M.; McClean, J. R.; McEwen, M.; Megrant, A.; Mi, X.; Mohseni, M.; Mruczkiewicz, W.; Mutus, J.; Naaman, O.; Neeley, M.; Neill, C.; Neven, H.; Niu, M. Y.; O'Brien, T. E.; Ostby, E.; Petukhov, A.; Putterman, H.; Quintana, C.; Roushan, P.; Rubin, N. C.; Sank, D.; Satzinger, K. J.; Smelyanskiy, V.; Strain, D.; Sung, K. J.; Szalay, M.; Takeshita, T. Y.; Vainsencher, A.; White, T.; Wiebe, N.; Yao, Z. J.; Yeh, P.; Zalcman, A. Hartree-Fock on a superconducting qubit quantum computer. *Science* **2020**, *369*, 1084−1089.

(46) Sparrow, C.; Martín-López, E.; Maraviglia, N.; Neville, A.; Harrold, C.; Carolan, J.; Joglekar, Y. N.; Hashimoto, T.; Matsuda, N.; O'Brien, J. L.; Tew, D. P.; Laing, A. Simulating the vibrational quantum dynamics of molecules using photonics. *Nature* **2018**, *557*, 660−667.

(47) Wang, C. S.; Curtis, J. C.; Lester, B. J.; Zhang, Y.; Gao, Y. Y.; Freeze, J.; Batista, V. S.; Vaccaro, P. H.; Chuang, I. L.; Frunzio, L.; Jiang, L.; Girvin, S. M.; Schoelkopf, R. J. Efficient Multiphoton Sampling of Molecular Vibronic Spectra on a Superconducting Bosonic Processor. *Phys. Rev. X* **2020**, *10*, 021060.

(48) Huh, J.; Guerreschi, G. G.; Peropadre, B.; McClean, J. R.; Aspuru-Guzik, A. Boson sampling for molecular vibronic spectra. *Nat. Photonics* **2015**, *9*, 615−620.

(49) Wang, Y.; Sager-Smith, L. M.; Mazziotti, D. A. Quantum Simulation of Bosons with the Contracted Quantum Eigensolver. *arXiv* **2023**, 2307.07088.

(50) Wang, C. S.; Frattini, N. E.; Chapman, B. J.; Puri, S.; Girvin, S. M.; Devoret, M. H.; Schoelkopf, R. J. Observation of Wave-Packet Branching through an Engineered Conical Intersection. *Phys. Rev. X* **2023**, *13*, 011008.

(51) Saha, D.; Iyengar, S. S.; Richerme, P.; Smith, J. M.; Sabry, A. Mapping Quantum Chemical Dynamics Problems to Spin-Lattice Simulators. *J. Chem. Theory Comput.* **2021**, *17*, 6713−6732.

(52) Cleland, W. W.; Kreevoy, M. M. Low-Barrier Hydrogen-Bonds and Enzymatic Catalysis. *Science* **1994**, *264*, 1887.

(53) Clark, S. M.; Lobser, D.; Revelle, M. C.; Yale, C. G.; Bossert, D.; Burch, A. D.; Chow, M. N.; Hogle, C. W.; Ivory, M.; Pehr, J.; Salzbrenner, B.; Stick, D.; Sweatt, W.; Wilson, J. M.; Winrow, E.; Maunz, P. Engineering the Quantum Scientific Computing Open User Testbed. *IEEE Transactions on Quantum Engineering* **2021**, *2*, 1−32.

(54) Braams, B. J.; Bowman, J. M. Permutationally invariant potential energy surfaces in high dimensionality. *Int. Rev. Phys. Chem.* **2009**, *28*, 577.

(55) Peláez, D.; Meyer, H.-D. The multigrid POTFIT (MGPF) method: Grid representations of potentials for quantum dynamics of large systems. *J. Chem. Phys.* **2013**, *138*, 014108.

(56) Kumar, A.; DeGregorio, N.; Ricard, T.; Iyengar, S. S. Graph-Theoretic Molecular Fragmentation for Potential Surfaces Leads Naturally to a Tensor Network Form and Allows Accurate and Efficient Quantum Nuclear Dynamics. *J. Chem. Theory Comput.* **2022**, *18*, 7243.

(57) Greene, S. M.; Batista, V. S. Tensor-Train Split-Operator Fourier Transform (TT-SOFT) Method: Multidimensional Non-adiabatic Quantum Dynamics. *J. Chem. Theory Comput.* **2017**, *13*, 4034−4042.

(58) Orús, R. A practical introduction to tensor networks: Matrix product states and projected entangled pair states. *Ann. Physics* **2014**, *349*, 117−158.

(59) Hackbusch, W.; Khoromskij, B. N. Tensor-product approximation to operators and functions in high dimensions. *J. Complex.* **2007**, *23*, 697−714.

(60) Wang, H.; Thoss, M. Multilayer formulation of the multiconfiguration time-dependent Hartree theory. *J. Chem. Phys.* **2003**, *119*, 1289−1299.

(61) DeGregorio, N.; Iyengar, S. S. Adaptive Dimensional Decoupling for Compression of Quantum Nuclear Wave Functions and Efficient Potential Energy Surface Representations through Tensor Network Decomposition. *J. Chem. Theory Comput.* **2019**, *15*, 2780−2796.

(62) Althorpe, S. C.; Fernandez-Alonso, F.; Bean, B. D.; Ayers, J. D.; Pomerantz, A. E.; Zare, R. N.; Wrede, E. Observation and Interpretation of a Time-Delayed Mechanism in the Hydrogen Exchange Reaction. *Nature* **2002**, *416*, 67.

(63) Colbert, D. T.; Miller, W. H. A Novel Discrete Variable Representation for Quantum-Mechanical Reactive Scattering Via the S-Matrix Kohn Method. *J. Chem. Phys.* **1992**, *96*, 1982.

(64) Kouri, D. J.; Huang, Y.; Hoffman, D. K. Iterated Real-Time Path Integral Evaluation Using a Distributed Approximating Functional Propagator and Average-Case Complexity Integration. *Phys. Rev. Lett.* **1995**, *75*, 49.

(65) Hoffman, D. K.; Nayar, N.; Sharafeddin, O. A.; Kouri, D. J. Analytic Banded Approximation for the Discretized Free Propagator. *J. Phys. Chem.* **1991**, *95*, 8299.

(66) Iyengar, S. S. Ab Initio Dynamics with Wave-Packets and Density Matrices. *Theor. Chem. Accts.* **2006**, *116*, 326.

(67) Ortiz, G.; Gubernatis, J. E.; Knill, E.; Laflamme, R. Quantum algorithms for fermionic simulations. *Phys. Rev. A* **2001**, *64*, 022319.

(68) Olmschenk, S.; Younge, K. C.; Moehring, D. L.; Matsukevich, D. N.; Maunz, P.; Monroe, C. Manipulation and detection of a trapped Yb[sup +] hyperfine qubit. *Phys. Rev. A* **2007**, *76*, 052314.

(69) Vatan, F.; Williams, C. Optimal quantum circuits for general two-qubit gates. *Phys. Rev. A* **2004**, *69*, 032315.

(70) Tucci, R. R. An introduction to Cartan's KAK decomposition for QC programmers. *arXiv* **2005**. DOI: 10.48550/arXiv.quant-ph/0507171

(71) Maslov, D. Basic circuit compilation techniques for an ion-trap quantum machine. *New J. Phys.* **2017**, *19*, 023035.

(72) Mølmer, K.; Sørensen, A. Multiparticle entanglement of hot trapped ions. *Phys. Rev. Lett.* **1999**, *82*, 1835.

(73) Maunz, P. High optical access trap 2.0. *Technol. Rep.* SAND2016-0796R, **2016**.

(74) Senko, C.; Smith, J.; Richerme, P.; Lee, A.; Campbell, W.; Monroe, C. Coherent imaging spectroscopy of a quantum many-body spin system. *Science* **2014**, *345*, 430−433.

(75) Jurcevic, P.; Hauke, P.; Maier, C.; Hempel, C.; Lanyon, B.; Blatt, R.; Roos, C. F. Spectroscopy of interacting quasiparticles in trapped ions. *Phys. Rev. Lett.* **2015**, *115*, 100501.